Virginia Tech – Wake Forest University

Center for Injury Biomechanics

CIB Report Number: WFU2008-020

FINAL REPORT

ARC Farside, Task 3: *Finite Element Modeling of the Carotid Artery*

PREPARED FOR

ARC Farside Committee

Final Report

PREPARED BY

Kerry Danelson, Scott Gayzik, Mao Yu, Stefan Duma, Joel Stitzel

Virginia Tech – Wake Forest University

Center for Injury Biomechanics

Wake Forest University School of Medicine

Medical Center Boulevard, Winston-Salem, NC 27157

Phone: (336) 716-5597, jstitzel@wfubmc.edu

October 8, 2008

Table of Contents

List of Tables

List of Figures

Abstract

Carotid artery injury has been attributed to direct impact to the neck as well as stretching of the artery as a result of extension of the neck. These injuries can be life-threatening because all of the blood supply to the brain travels through the carotid or vertebral arteries. To investigate possible mechanisms of injury given a lateral impact loading scenario, a regional finite element model of the neck was created. This model includes the carotid arteries developed in a previous study, an existing Finite Element Model (FEM) of the head and spine down to the level of T1, and a neck and shoulder fascia. This model was constrained by motion determined by modeling four postmortem human subject sled tests of a lateral impact using the Total Human Model for Safety (THUMS). The configurations tested were high and low belt placements given high and low delta-v for each belt placement. The regional neck model completed three of the four load configurations but there were consistent error terminations of the model in the high belt, high delta-v load configuration. Given the model results and the THUMS model results, it was estimated that this failed configuration would result in maximal compressive loading of the ipsilateral vessel. The high delta-v, low belt configuration resulted in maximal extension of the neck. This load condition would result in the highest likelihood of extension injuries to the contralateral vessel. Of the load configurations that ran to completion, the only one that did not predict injury was the low belt, low delta-v test.

1. Introduction

Carotid artery injury has been attributed to direct impact to the neck as well as stretching of the artery as a result of extension of the neck [1, 2]. Injury to the carotid artery can be life threatening because these vessels, combined with the vertebral arteries, provide all of the blood supply to the brain. These injuries can begin with intimal tears that create a disruption to the vessel. From an intimal disruption, the vessel can become injured through occlusion through platelet aggregation, dissection of the intima, aneurysm, and intramural hematoma [3-5]. Approximately 7000 cases of internal artery dissection occur in the United States per year [6, 7]. In a farside crash, a common mechanism of injury is significant movement of the occupant due to the three point restraint system [8]. There is significant interest in the protective capabilities of a four point belt system and other torso restraint systems using postmortem human subjects (PMHS) and finite element models (FEM). However, there are few finite element models in the literature that have attempted to model this method of injury to these important vessels. To test these mechanisms of injury, this study correlated a regional model of the neck and carotid arteries to the results of PMHS impact tests. The model developed from this study

2. Methods

This study focused on the development of a regional head, neck and carotid model to examine the response of the carotid artery given lateral impact loading conditions. The methodology for this study can be broken into three components. The first is an initial model assessment, where the separate parts of the model were examined and initially put together. The next step was establishing boundary conditions of the model by using the Total Human Model for Safety (THUMS) to establish a realistic kinematic given a crash impulse. The last step was integrating these boundary conditions into the existing model and completing the model to assess the response of the model under four different load conditions. These steps will be examined in further detail in the following paragraphs.

2.1. Initial Model Assessment

The first step in the regional model creation was assessing the components of the model that were going to be used and completing an initial compilation of these components. The finite element software selected for this study was LSDYNA (LSTC, Livermore, CA). This regional model of the carotid integrates an existing head and spine model developed by Kleinburger et al [9] with the carotid material model and geometry developed by Gayzik et al [10]. Before all of the necessary components were added to fully model a cadaver impact study, the model had to be examined step by step.

The first step was to integrate the geometry of the carotid into a neck composed solely of fascia to demonstrate the response of the carotid given the correct geometry and the validated material model from Gayzik et al. This model had neck fascia that was the same material and the same geometry as the THUMS neck fascia. The carotid artery was created from a CT scan of a 57 year old male subject [10]. The crash scenario was modeled as a bent indenter that impacted the side of the neck at the level of the carotid bifurcation. This structure approximated a roped seatbelt. The indenter had a boundary condition of sinusoidal motion while there were locked nodes on the inferior aspect of the

neck model and the medial space in the neck that approximated the vertebral column. The key components of this model are highlighted in Table 2.1-1 and illustrated in Figure 2.1-1 and Figure 2.1-2.

Figure 2.1-1: Initial neck regional model with neck fascia, carotid arteries and a seatbelt indenter.

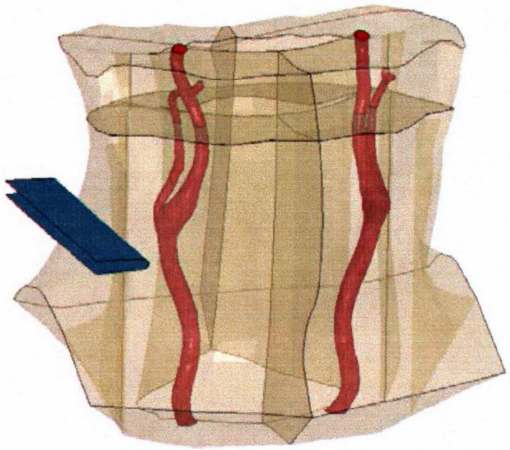

Figure 2.1-2: Initial neck regional model, transparent fascia for visualization of the carotid artery placement.

Table 2.1-1: Summary of key model properties, initial regional model

Materials	Neck Fascia and musculature	*Mat_Viscoelastic
	Carotid	*Mat_Simplified_Rubber
	Indenter	*Mat_Rigid
Contacts	Neck to Carotid	Auto_Surface_to_Surface
	Neck top to neck bottom	Tied Nodes
Boundary	Locked nodes	Inferior plane, medial vert body space
	Indenter	Sinusoidal Motion

This model was run and the resulting strains in the shells around the carotid artery were evaluated. This model did not incorporate the bony structures of the neck, the inertial response of the head and the corresponding response of the opposite side of the neck. Due to these limitations, it was determined that a model that incorporates these aspects needed to be developed to evaluate the carotid response on both sides of the neck. This model could study the compression of the carotid on the ipsolateral side and the extension of the carotid on the contralateral side.

To more accurately model an impact scenario, there were several modifications to the existing model. The first was the addition of the Kleinberger neck model. This model was developed to study cervical spine mechanics in frontal impact scenarios. The first step in this integration was translating this model into current Dyna code. From that point, the unit system was translated to m-N-kg-s. This model is pictured below in Figure 2.1-3 and Figure 2.1-4. As shown by these figures, the main cervical anatomy modeled are the vertebral bodies from C1 to T1, a head mass that has the geometry of an anthropometric test device (ATD), the primary ligaments that connect the vertebral bodies, and the facet joints. When this model was combined with the existing neck

regional model, the neck fascia was too wide for the Kleinberger head, as illustrated in Figure 2.1-5 and Figure 2.1-6.

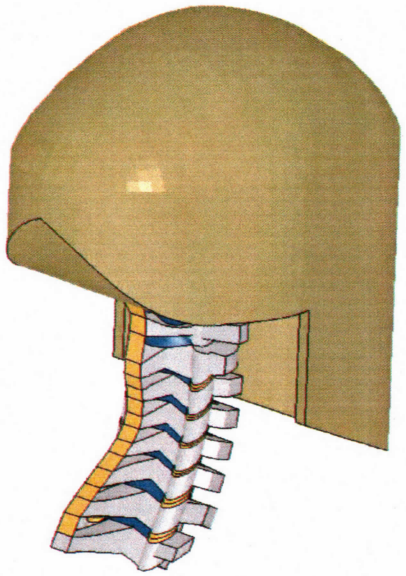

Figure 2.1-3: Rear oblique view of the Kleinberger neck model

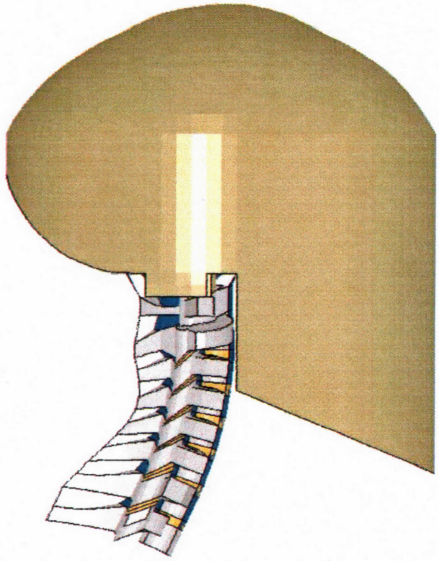

Figure 2.1-4: Right side view of the Kleinberger neck model

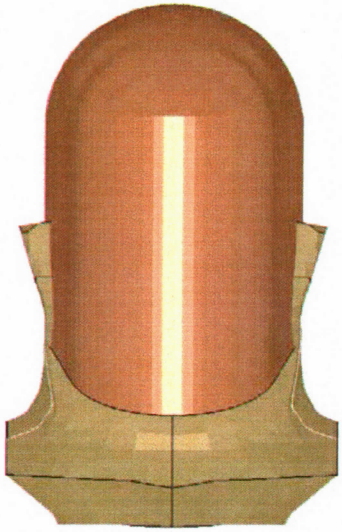

Figure 2.1-5: Front view of the initial neck model with the head and spine.

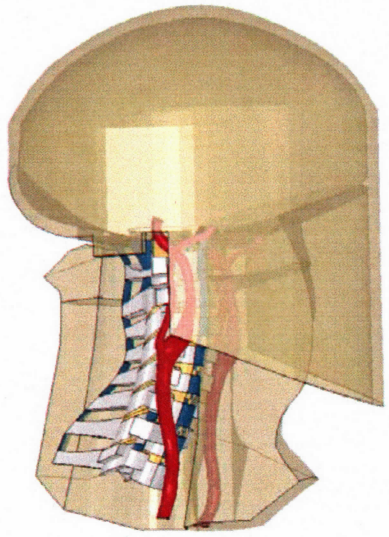

Figure 2.1-6: Oblique view with the right neck fascia removed and transparent head and fascia to illustrate the spine and carotid placement.

To make a more anatomically accurate model, a new neck fascia was created to have the same contours as the head in the spine model. Additionally, measurements taken from CT were used to properly place the carotid arteries in relation to the vertebral bodies [11]. Figure 2.1-7 and Figure 2.1-8 illustrate the new neck fascia integrated with the Kleinberger neck. The locations of the carotid

arteries, in relation to the vertebral bodies, are shown in Figure 2.1-9 and Figure 2.1-10. The important model characteristics are shown in

Table 2.1-2

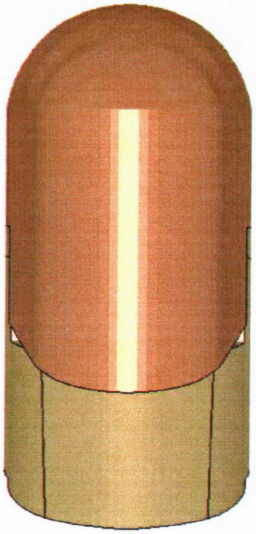

Figure 2.1-7: Kleinberger neck integrated with revised neck fascia.

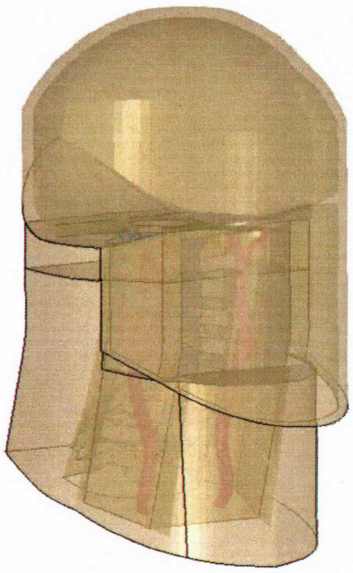

Figure 2.1-8: Oblique view of the Kleinberger neck integrated with the revised neck fascia, fascia and head are transparent.

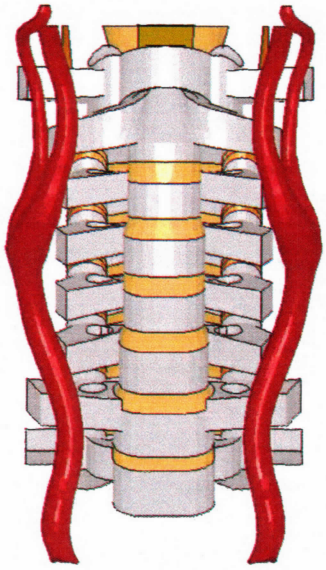

Figure 2.1-9: Front view of carotid placement, with select ligaments removed for clarity.

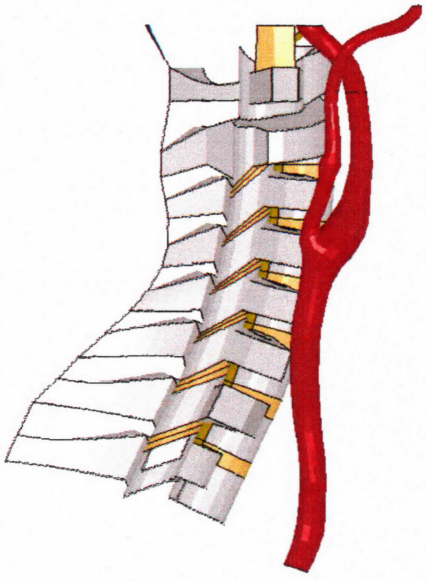

Figure 2.1-10: Right view of carotid placement, with select ligaments removed for clarity.

Table 2.1-2: Model parameters for the first version of the integrated head, spine, and neck model.

Materials	Neck fascia and musculature	*Mat_Elastic
	Carotid	*Mat_Simplified_Rubber
	Ligaments, Disks	*Mat_Elastic
	Vertebral bodies, Head	*Mat_Rigid
Contacts	NHTSA neck	Preserve contacts
	Top of neck to head	Constrained extra nodes
	Neck to carotid	Tied surf to surf
	Vertebral bodies to neck	Auto surf to surf
Boundaries	Locked nodes	Bottom of neck to T1
	T1	Prescribed motion

Once this step was complete, initial runs of the model were conducted to evaluate the response of the spine model in a side impact loading scenario. For these impacts, acceleration data from MCW far side PMHS tests were used as the boundary conditions. Figure 2.1-11 shows all the plots of the initial load configurations for the four load conditions of low belt and low delta-v, low belt and high delta-v, high belt and low delta-v, and high belt and high delta-v.

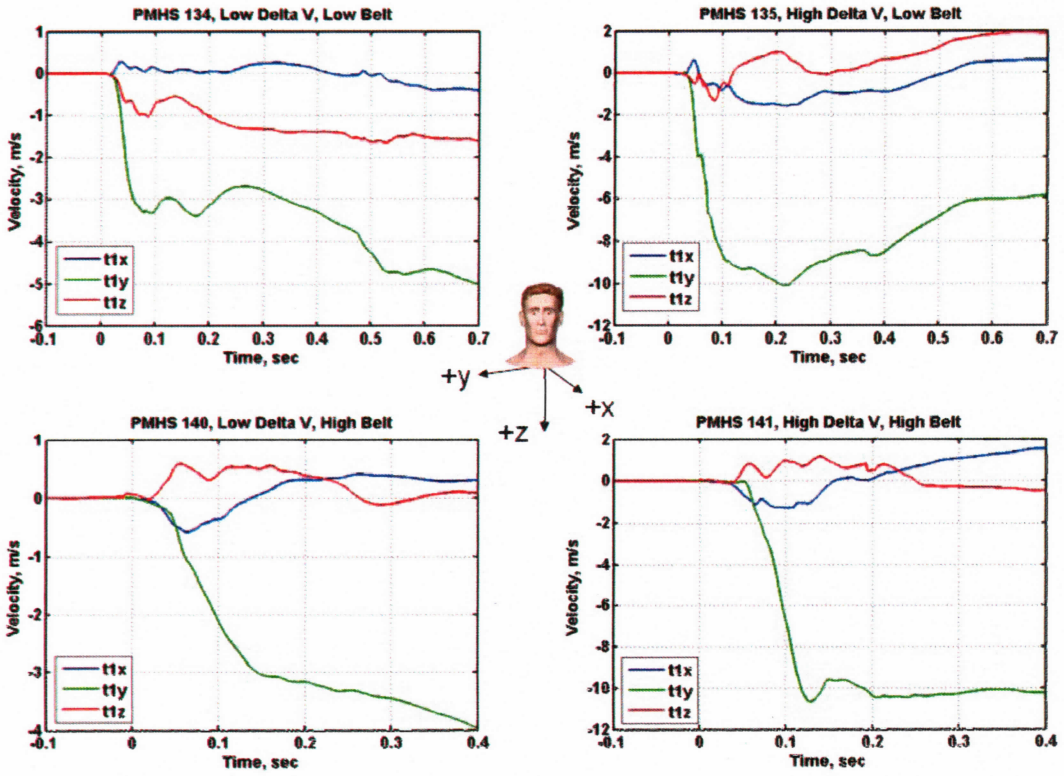

Figure 2.1-11: Boundary conditions for T1 from the MCW tests. The blue line is T1 x velocity (m/s), the green line is T1 y velocity (m/s), and the red line is T1 z velocity (m/s).

The T1 velocity data from the tests was applied as a velocity to T1 in the model. The bottom of the neck was constrained to move in the same manner as T1. The top of the neck was coupled to the bottom of the head. During this phase of the model development, different versions of the material models used for the neck fascia and ligaments were evaluated over a range of load conditions.

2.2. Kinematic Modeling Using THUMS

Given the response of the Kleinberger neck at high delta-V, the initial model configuration was determined to be unstable and without a biofidelic response of the head and neck. To address this issue, the boundary conditions to be modeled were used as inputs to the Total Human Model for Safety (THUMS). The acceleration recorded for the seat in the MCW tests was applied to the seat as the boundary condition for the THUMS model. The THUMS model was placed in a similar sled configuration as the test configuration. This configuration was reconstructed from diagrams and descriptions in Pintar et al [12]. In the THUMS model, there were nodes selected on each of the cervical vertebral bodies, the first thoracic vertebral body, the shoulder attachment of the modeled seatbelt, and a node on the seatbelt located at the sternum. The displacements of these nodes were recorded for each test configuration. These displacement files were then used as inputs for the final model.

2.3. Final Model Parameters

The final model used the neck fascia contoured to the head of the neck model as described as the final configuration for the first version of the regional model. The ligaments and the intervertebral discs were removed because each vertebral body was constrained. A shoulder structure that was modified from the THUMS shoulder geometry was added to the model with the same material properties as the neck fascia. This addition was to prevent the seatbelt from slipping under the neck. A seatbelt segment was also added to the final model. This belt went from an upper attachment point, just like the full THUMS model, and terminated at the approximate level of the sternum. The location of the upper attachment point was measured from the level of T1 and comparable to the location of the anchor point in the PMHS tests. The sternum attachment point was also estimated based on the similar location on the THUMS model. Figure 2.3-2 and Figure 2.3-1 show the complete model given a high belt configuration. Table 2.3-1 lists the key components of the final model.

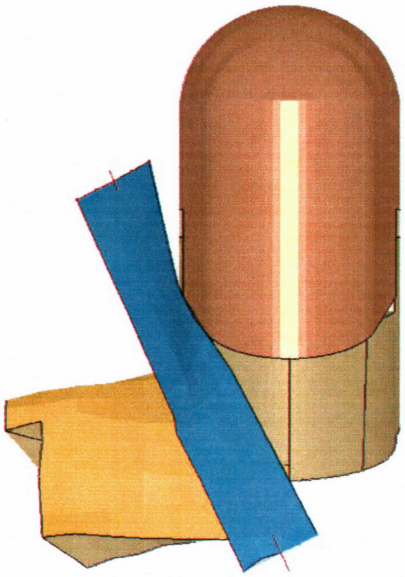

Figure 2.3-1: Front view of the final version of the neck regional model.

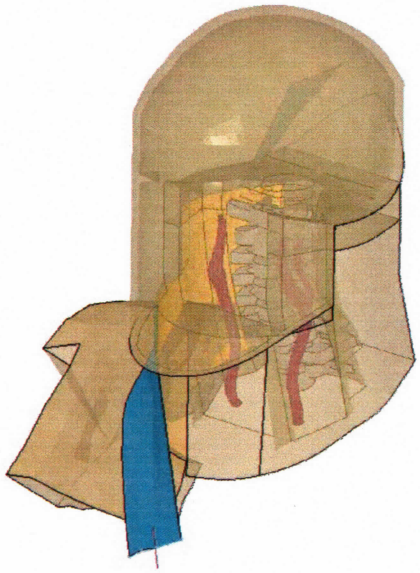

Figure 2.3-2: Oblique view with the fascia removed and transparent head and fascia.

Table 2.3-1: Model parameters for the final version of the integrated head, spine, and neck model.

Materials	Neck fascia and musculature	*Mat_Elastic
	Carotid	*Mat_Simplified_Rubber
	Ligaments, Disks	REMOVED
	Vertebral bodies, head	*Mat_Rigid
	Seatbelt	*Mat_seatbelt
Contacts	NHTSA neck	Remove all existing
	Top of neck to head	Constrained extra nodes
	Neck to Carotid	Shared nodes
	Vertebral bodies to Neck	Auto surf to surf
	Seatbelt to neck	Auto surf to surf
	Bottom of neck to T1	Constrained extra nodes
Boundaries	All Vertebral bodies, Seatbelt	Displacement from THUMS

The model was run given 4 conditions based on PMHS test configurations as shown in the test matrix in Table 2.3-2. From Pintar et al [12], an intimal tear occurred in the PMHS test that experienced high belt loading at both high and low speeds. Since multiple tests were conducted on the same PMHS, the time of the carotid artery injury is unknown.

Table 2.3-2: Test Matrix for the model

PMHS Test No.	Belt Position	Delta-V
134	Low	Low
135	Low	High
140	High	Low
141	High	High

3. Results

There were several steps before the final version of the model; therefore, there were several intermediate results that will be discussed in this section. The first segment was an initial model assessment to determine the response of the Kleinberger neck [9]. The second was kinematic modeling of the neck using the THUMS model. The final step is integration of the displacement data from the THUMS model with the

3.1. Initial Model Assessment

The initial model assessment demonstrated instability of the Kleinberger neck in a lateral impact scenario. Also, the Kleinberger neck demonstrated a lack of biofidelic response of the spinal column. Finally, the neck had no shoulder; therefore, the low belt configuration did not properly interact with the model. Figure 3.1-1 and Figure 3.1-2 demonstrate the failure of the spinal column due to interaction between the vertebral bodies and the low belt configuration

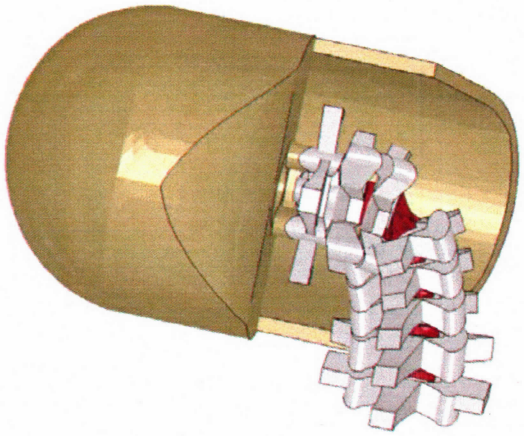

Figure 3.1-1: The response of the Kleinberger neck given a lateral impact scenario

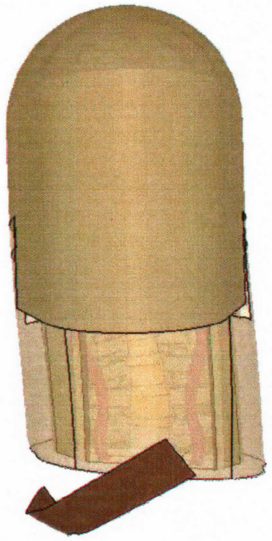

Figure 3.1-2: Low belt missing the first version of the combined model

These problems were a result of the geometry of the existing head and neck model. Specifically, the vertebral bodies had significant interaction between the lateral edges which prevented reasonable lateral flexion. Additionally, the ligament structures in the model were more efficient at constraining anterior to posterior motion rather than lateral motion. Given these results, it was determined that the motion of the vertebral bodies would have to be determined in another manner. The existing THUMS finite element model was selected as a method of obtaining displacement data for each vertebral body.

3.2. Kinematic Modeling Using THUMS

The THUMS model was taken and seated in the same sled configuration as the PMHS subjects used in data collection. All of the loading scenarios ran to completion with

qualitative improvements of the model response. The time at maximum extension of the THUMS model was noted in Table 3.2-1 for comparison with the regional carotid artery models. Figure 3.2-1 and Figure 3.2-2 illustrate the THUMS model in the high and low belt configurations. The model response at the time of maximum extension is shown in Figure 3.2-3 to Figure 3.2-6 for each test configuration. This response qualitatively matched the PMHS test results.

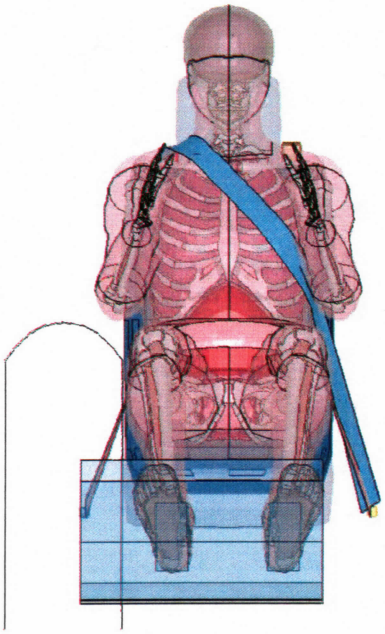

Figure 3.2-1: THUMS model with the low belt configuration.

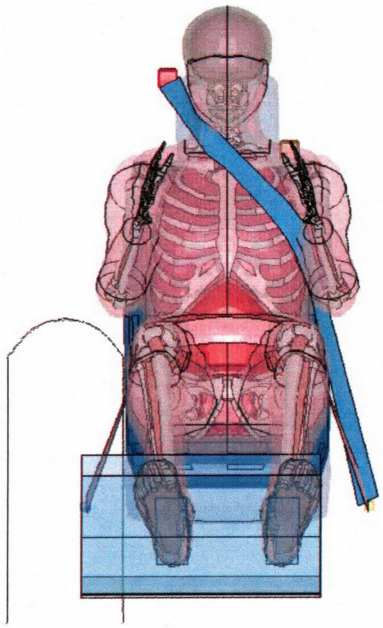

Figure 3.2-2: THUMS model with the high belt configuration.

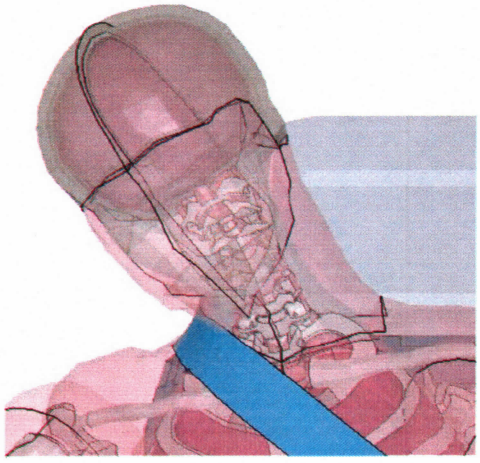

Figure 3.2-3: THUMS model at maximum neck extension, low belt and low delta-v

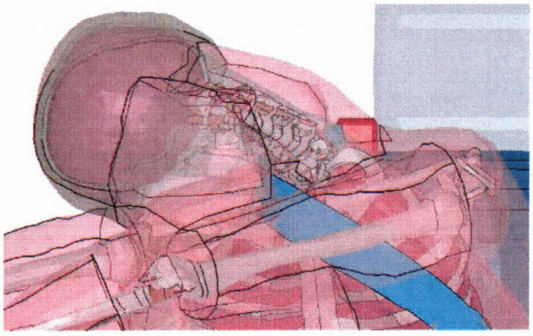

Figure 3.2-4: THUMS model at maximum neck extension, low belt and high delta-v

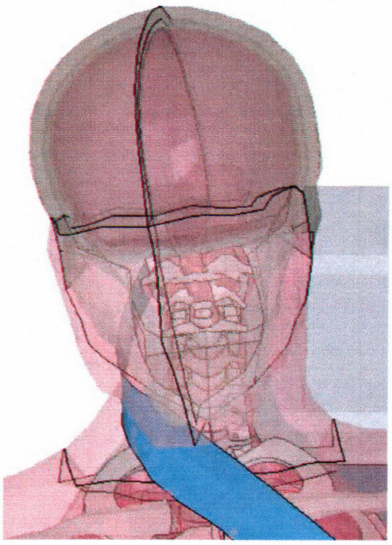

Figure 3.2-5: THUMS model at maximum neck extension, high belt and low delta-v

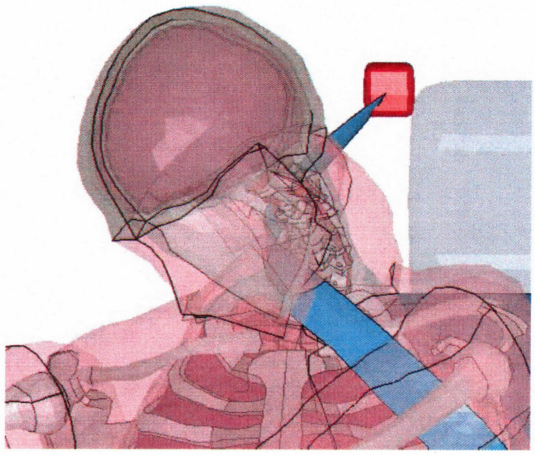

Figure 3.2-6: THUMS model at maximum neck extension, high belt and high delta-v

Table 3.2-1: Time of maximum neck extension of the THUMS model

Test Configuration	Time of Maximum extension
Low Belt, Low Delta-V	140 ms
Low Belt, High Delta-V	135 ms
High Belt, Low Delta-V	110 ms
High Belt, High Delta-V	120 ms

3.3. Final Model Parameters

Using the THUMS model results as inputs for the final version of the combined neck and carotid model, the 4 load configurations were examined. The first measure of the possibility of injury to the carotid was the largest maximum principal strain value measured in any element of the carotid artery shells. These values are listed in Table 3.3-1. As this table illustrates, the highest strain value out of the models that ran to completion was in the low belt, high delta-V configuration. There is a trend between the low belt configurations in that as the delta-V increases, the maximum stain value increases. This trend was also postulated to apply to the high belt configurations.

Table 3.3-1: Maximum principal strain values for each test configuration

Test Configuration	Maximum Principal Stain	Time of Maximum Stain
Low Belt, Low Delta-V	0.3182	136.5 ms
Low Belt, High Delta-V	1.5874	126.0 ms
High Belt, Low Delta-V	1.2884	136.5 ms
High Belt, High Delta-V	Error Termination	Error Termination

To examine the location of the higher strain values in the carotid artery, the fringe plot function in LS-Prepost (LSTC, Livermore, CA) was used to graphically illustrate the location of high strain values. The areas of red, orange and yellow have higher strain.

Areas in blue and green have a lower strain value. To have these fringe plots reflect the same relative scale, the maximum strain value (illustrated by dark red) was set as 1.3. This was based on the maximum value of 1.5874 recorded for the Low Belt, High Delta-V configuration. The minimum value (illustrated by darker blue) was set as 0.

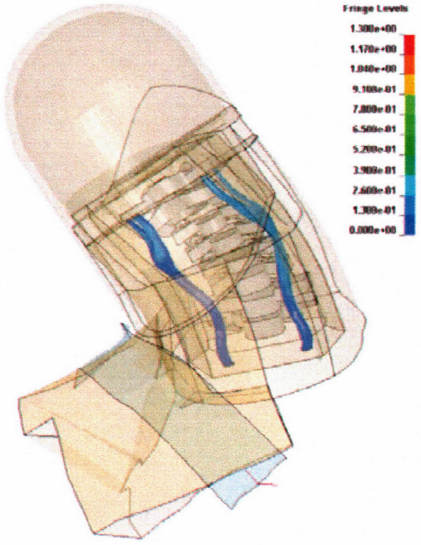

Figure 3.3-1: Fringe plot of the Low Delta-V, Low Belt impact configuration. This is at the time of the maximum strain, 125 ms.

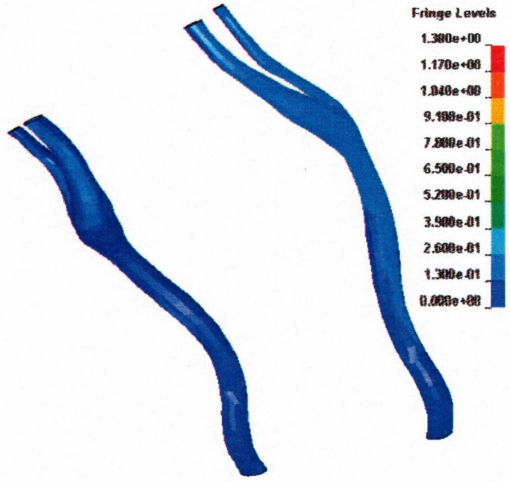

Figure 3.3-2: Close up of the same time point and the same approximate orientation with the carotid arteries isolated.

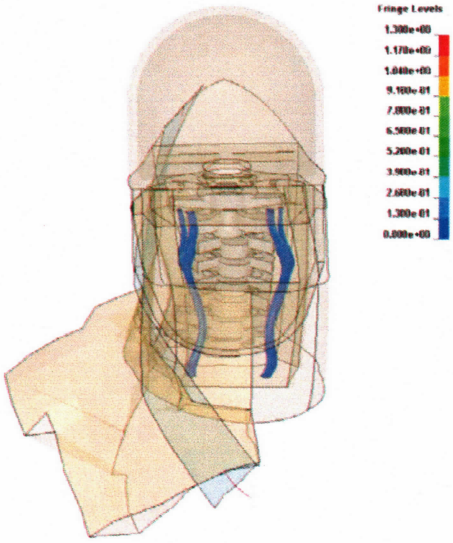

Figure 3.3-3: Fringe plot of the Low Delta-V, High Belt impact configuration. This is at the time of the maximum strain, 125 ms.

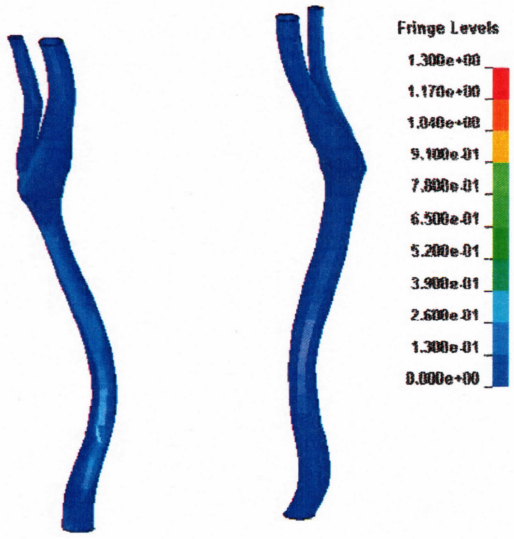

Figure 3.3-4: Close up of the same time point and the same approximate orientation with the carotid arteries isolated

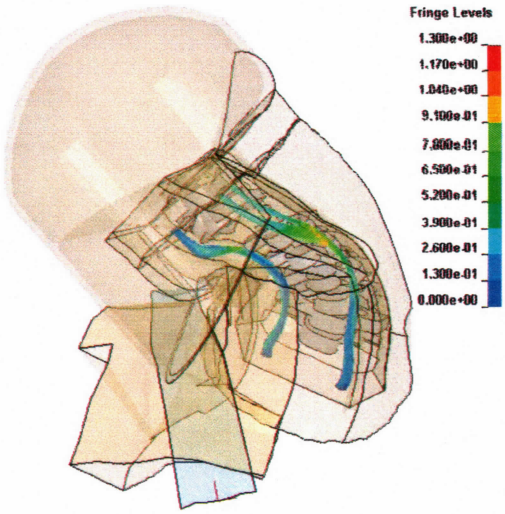

Figure 3.3-5: Fringe plot of the High Delta-V, Low Belt impact configuration. This is at the time of the maximum strain, 125 ms.

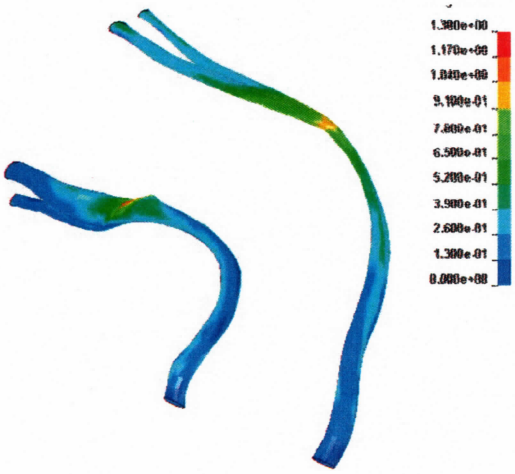

Figure 3.3-6: Close up of the same time point and the same approximate orientation with the carotid arteries isolated

These figures illustrate the low levels of strain in the low delta-V configurations, especially the low delta-V, low belt configuration shown in Figure 3.1-1 and Figure 3.3-2. The high belt, low delta-V plot, Figure 3.3-3 and Figure 3.3-4, showed higher strains than the low delta-V, low belt plot, but lower strains than the low belt, high delta-V plot, Figure 3.3-5 and Figure 3.3-6. These figures also show that even though there were isolated elements in the high belt, low delta-v configuration that achieved a fairly high strain, there were not many elements that experienced higher strains.

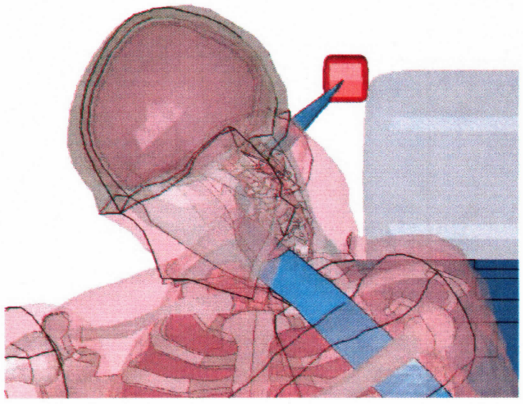

Figure 3.3-7: THUMS results, High delta-V, High belt configuration

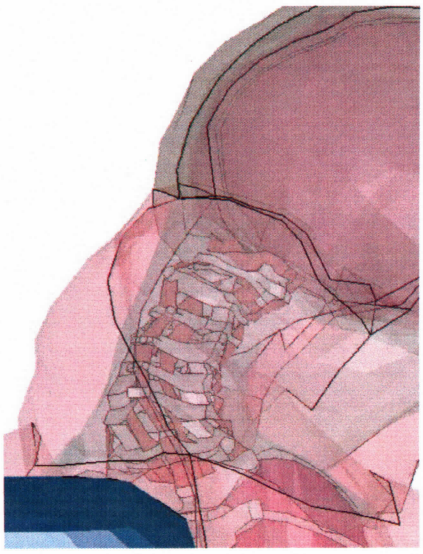

Figure 3.3-8: Close up view of the High Delta-V, high belt THUMS results

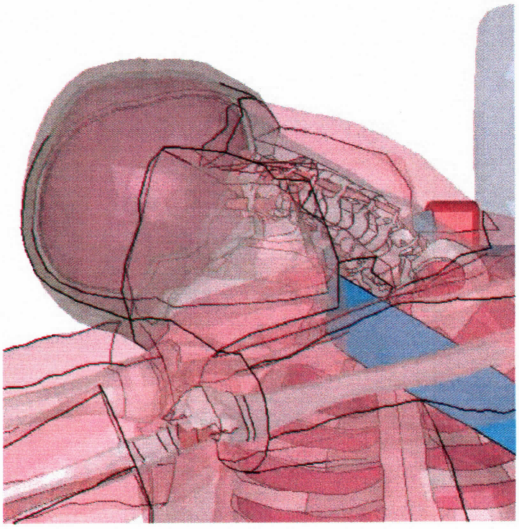

Figure 3.3-9: THUMS results, high delta-V, low belt configuration

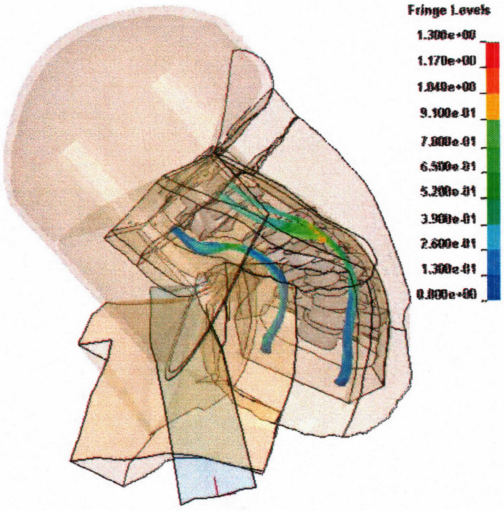

Figure 3.3-10: Version 2 model results, high delta-V, low belt

Next, to hypothesize the potential outcome for the high belt, high delta-v configuration the results from the THUMS model were compared between the belt configurations and given a high delta-v. Figure 3.3-7 and Figure 3.3-8 illustrate the loading scenario that the regional model failed to run to completion in the THUMS model. When compared to Figure 3.3-9 and Figure 3.3-10 there is significantly less extension of the spine in the high belt configuration. From these results it can be concluded that the high belt, high delta-V configuration will have less neck extension on the side contralateral to the belt than the low belt, high delta-V configuration. However, the high delta-V, high belt neck configuration will have more compression of the neck fascia and carotids between the belt and the vertebral bodies.

4. Discussion

The resulting neck model illustrated several trends in the response of the carotid artery given a lateral impact and variable speeds and belt positions. The primary trend seen in the results was the compression of the ipsolateral vessel, with respect to the belt, and stretching of the vessel on the contralateral side. Based on Stemper et al, the strain to failure for the intima is approximately 0.40 strain and to total vessel failure it is 0.60 strain [13]. Based on these values, at least one element in the high belt and low delta-v, and low belt and high delta-v cases exceeded this limit. Based on the THUMS modeling results, it is estimated that the high belt, high delta-v configuration would also have at least one element exceeding this value.

This model also demonstrated the need for continued development of neck models for lateral impact scenarios. The base neck model used for model development was validated solely in frontal flexion; therefore, it was unstable given a lateral impact. The THUMS model was then used to determine a more biofidelic neck response for the regional neck model. Another limitation of the regional model is the basic geometry used in the model. The head and vertebral bodies are relatively square and lack true

anatomical detail. The THUMS model, which was more anatomically accurate, had a more accurate model response given the loading scenario. Another limitation introduced with the geometry of the model used was the angular interfaces between structures. Again, this limited the ability of the model to replicate a biofidelic response.

5. Conclusions

To determine the possible effect of a four point style restraint in a farside crash configuration, a regional model of the neck and carotid artery was created. This model determined the strain in the carotid arteries given a range of impact severities and seatbelt configurations. Given the model response and the hypothesized strain to failure of the carotid artery, the carotid artery would have been injured in all of the tests except the low belt, low delta-v configuration. More importantly, the model illustrated that given a low belt configuration, the occupant was more likely to injure the contralateral vessel via an extension type injury. Given a high belt configuration, the occupant was more likely to injure the ipsolateral vessel via compression of the vessel between the seatbelt and the vertebral bodies.

6. References

[1] G. S. Rozycki, L. Tremblay, D. V. Feliciano, K. Tchorz, A. Hattaway, J. Fountain, and B. J. Pettitt, "A prospective study for the detection of vascular injury in adult and pediatric patients with cervicothoracic seat belt signs," *J Trauma,* vol. 52, pp. 618-23; discussion 623-4, Apr 2002.

[2] G. P. Sinson, N. Yoganandan, F. A. Pintar, R. Morgan, D. Maiman, K. Brasel, and T. A. Gennarelli, "Carotid artery trauma in motor vehicle crashes: Investigation of the local tensile mechanism," in *IRCOBI Conference*, Lisbon, Portugal, 2003, pp. 207-216.

[3] W. L. Biffl, E. E. Moore, P. J. Offner, and J. M. Burch, "Blunt carotid and vertebral arterial injuries," *World J Surg,* vol. 25, pp. 1036-43, Aug 2001.

[4] M. T. Haneline and G. N. Lewkovich, "An analysis of the etiology of cervical artery dissections: 1994 to 2003," *Journal of Manipulative and Physiological Therapeutics,* vol. 28, pp. 617-622, 2005.

[5] W. I. Schievink, "Spontaneous dissection of the carotid and vertebral arteries," *N Engl J Med,* vol. 344, pp. 898-906, Mar 22 2001.

[6] M. T. Haneline, A. C. Croft, and B. M. Frishberg, "Association of internal carotid artery dissection and chiropractic manipulation," *Neurologist,* vol. 9, pp. 35-44, Jan 2003.

[7] W. I. Schievink, B. Mokri, and W. M. O'Fallon, "Recurrent spontaneous cervical-artery dissection," *N Engl J Med,* vol. 330, pp. 393-7, Feb 10 1994.

[8] H. Gabler, K. H. Digges, B. N. Fildes, and L. Sparke, "Side Impact injury risk for belted far side passenger vehicle occupants," in *SAE World Congress, Paper #2005-01-0287*: Society of Automotive Engineers, Warrendale, PA, 2005.

[9] M. Kleinberger, "Application of Finite Element Techniques to the Study of Cervical Spine Mechanics," in *37th Strapp Car Crash Conference*: SAE, Warrendale, PA, 1993.

[10] F. Gayzik, J. Tan, S. Duma, and J. Stitzel, "Mesh development for a finite element model of the carotid artery," in *Biomedical Sciences Instrumentation Rocky Mountian Bioengineering Symposium*, Terre Haute, IN, 2006, pp. 187-192.

[11] C. C. Lambert, F. S. Gayzik, and J. D. Stitzel, "Characterization of the carotid and adjacent anatomy using non-contrast CT for biomechanical model development," *Biomed Sci Instrum,* vol. 43, pp. 330-5, 2007.

[12] F. A. Pintar, N. Yoganandan, B. D. Stemper, O. Bostrom, S. W. Rouhana, K. H. Digges, and B. N. Fildes, "Comparison of PMHS, WorldSID, and THOR-NT responses in simulated far side impact," *Stapp Car Crash J,* vol. 51, pp. 313-60, Oct 2007.

[13] B. D. Stemper, M. R. Stineman, N. Yoganandan, F. A. Pintar, G. P. Sinson, and T. A. Gennarelli, "Mechanical Characterization of Internal Layer Failure in the Human Carotid Artery," in *IRCOBI*, Prauge, Czech Republic, 2005, pp. 269-277.